ChemComm

COMMUNICATION

View Article Online
View Journal | View Issue

Cite this: *Chem. Commun.*, 2022, **58**, 13019

Received 12th August 2022,
Accepted 28th October 2022

DOI: 10.1039/d2cc04497h

rsc.li/chemcomm

Dynamics of the alkyne → copper(I) interaction and its use in a heteroleptic four-component catalytic rotor†

Suchismita Saha,[a] Sohom Kundu,[a] Pronay Kumar Biswas,[a] Michael Bolte[b] and Michael Schmittel*[a]

The HETPYNE (HETeroleptic Phenanthroline and alkYNE metal) and DABCO·(zinc porphyrin)$_2$ interactions were used to assemble the four-component nanorotor ROT-1 that exhibited a highly dynamic alkyne → copper(I) dissociation (k_{298} = 240 kHz) at 298 K. Quantitative click reaction transformed ROT-1 into the new rotor ROT-2 (k_{298} = 77 kHz) with a triazole → copper(I) linkage thus opening perspectives for bioorthogonal click strategies to biohybrid machinery.

Inspired by nanomechanical motions[1] in biological machines,[2–4] scientists have developed an enormous interest in the development of artificial molecular devices.[5–8] Among them, molecular motors,[9–11] rotors,[12] shuttles,[13–15] tweezers,[16–18] turnstiles,[19] muscles,[20] elevators,[21] pumps,[10] walkers[22] *etc.*[5–8] are well studied. Though numerous examples of artificial covalent molecular devices are known in the literature,[5–8] evolution toward multicomponent artificial machineries still represents a major challenge due to the limited amount of dynamic orthogonality in hetero-assemblies.[23,24]

For designing artificial multicomponent rotors, orthogonal dynamic interactions are a key requirement.[25] To the best of our knowledge, all literature known dynamic interactions that have been used to construct artificial multicomponent rotors are derived from H-bonding or *N,O*-donor[19] metal interactions.[26–30] Clearly, development of any new dynamic interaction will open further opportunities. Here, we demonstrate for the first time a supramolecular assembly and a rotor built on the dynamic alkyne → copper(I) interaction.[31,32] Specifically, we designed a four-component supramolecular assembly and nanorotor based on the heteroleptic Cu$^+$-phenanthroline alkyne (HETPYNE: HETeroleptic Phenanthroline and alkYNE metal) complexation (Fig. 1). Addition of stoichiometric quantities of azide to the rotor afforded the new class of a Cu$^+$-triazole rotor through an *in situ* copper(I) catalysed click reaction.

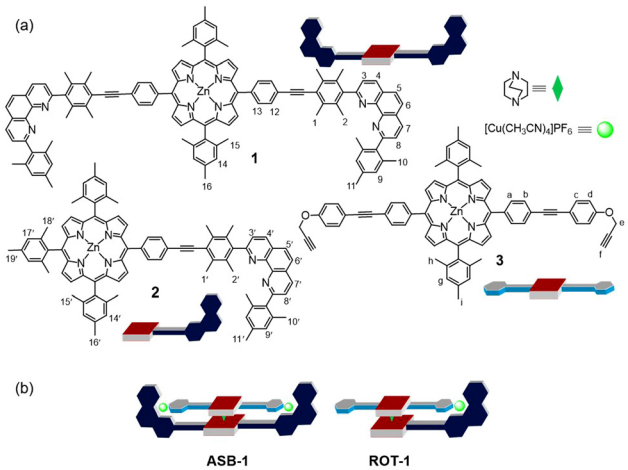

Fig. 1 (a) Chemical structure and cartoon representation of the ligands **1**, **2**, **3** and DABCO. (b) Cartoon representation of the four-component assembly **ASB-1** and nanorotor **ROT-1**.

For our study, we decided to use the phenanthroline-appended zinc(II) porphyrin ligands **1** or **2** as stator. Bulky aryl groups[33] at the 2,9-position of the phenanthroline phenAr$_2$ are essential to avoid the unwanted formation of the corresponding homoleptic Cu$^+$ complexes.[34–36] In order to design rotator **3**, we performed a few model experiments to evaluate the binding of a terminal ethynyl group to [Cu(phenAr$_2$)]$^+$. Mixing of **4**, **5** and [Cu(CH$_3$CN)$_4$]PF$_6$ in 1 : 1 : 1 ratio (2.5 mM each) in CD_2Cl_2 accomplished quantitative formation of **C1** = [Cu(**4**)(**5**)]$^+$ (Fig. 2a). In the ^{1}H NMR, a downfield shift of all phenanthroline protons indicated binding of **5** to [Cu(**4**)]$^+$, for instance, proton 4″-H shifted from 8.67 to 8.74 ppm and 5″-H from

[a] *Center of Micro and Nanochemistry and (Bio)Technology, Organische Chemie I, Universität Siegen, Adolf-Reichwein-Str. 2, Siegen D-57068, Germany. E-mail: schmittel@chemie.uni-siegen.de; Tel: +49(0) 2717404356*

[b] *Institut für Organische Chemie und Chemische Biologie, Johann Wolfgang Goethe-Universität, Max-von-Laue Strasse 7, Frankfurt am Main D-60438, Germany*

† Electronic supplementary information (ESI) available: Experimental procedures, compound characterizations, spectral data, NMR titration, and VT-^{1}H-NMR kinetics. CCDC 2199510. For ESI and crystallographic data in CIF or other electronic format see DOI: https://doi.org/10.1039/d2cc04497h

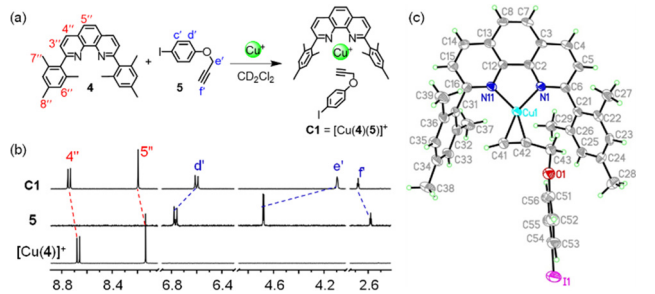

Fig. 2 (a) Formation of model complex **C1**. (b) Partial ^{1}H NMR (400 MHz, 298 K) of $[Cu(\mathbf{4})]^+$, **5** and **C1** in CD_2Cl_2 (2.5 mM). (c) X-ray crystal structure of complex **C1**. Carbons are shown in light grey; H, light green; N, blue; O, red; Cu^+, cyan and I, violet.

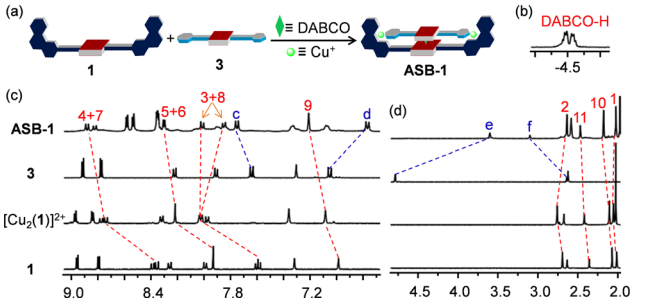

Fig. 3 (a) Cartoon representation of the four-component self-assembly leading to the formation of **ASB-1**. (b) DABCO-H signal of **ASB-1** in ^{1}H NMR (CD_2Cl_2, 400 MHz, 298 K). Partial ^{1}H NMR (CD_2Cl_2, 400 MHz, 298 K) of **1**, $[Cu_2(\mathbf{1})]^{2+}$, **3** and **ASB-1** showing the (c) aromatic and (d) aliphatic region.

8.14 to 8.20 ppm (Fig. 2b). In contrast, protons d′-H (from 6.77 to 6.60 ppm) and e′-H (from 4.68 to 4.09 ppm) of the ethynyl ligand **5** shifted upfield upon its complexation to $[Cu(\mathbf{4})]^+$, due to the shielding of these protons by the π-ring current of the mesityl groups. On the other hand, despite being in the shielding region of a strong π-electron cloud, the downfield shift of proton f′-H (from **5** to **C1**: 2.58 to 2.68 ppm) validated the ethynyl binding to the Cu^+ center. Single crystal X-ray analysis of **C1** revealed a triclinic crystal system with the space group $P\bar{1}$ (ESI,† Fig. S27). Importantly, it clearly demonstrated the side-on binding of Cu^+ to both ethynyl carbons whereas there was no binding visible between oxygen and Cu^+ center (Fig. 2c). The solid state structure disclosed the bond lengths of Cu(1)–C(41), Cu(1)–C(42), Cu(1)–N(11) and Cu(1)–N(1) to be 1.958(5) Å, 1.969(4) Å, 2.002(3) Å and 2.013(3) Å, respectively. The angle between the planes defined by N(1)–Cu(1)–N(11) and C(41)–Cu(1)–C(42) was determined as 16°. This geometry around the copper(I) center is not very common. From an NMR titration, the binding constant of **5** to $[Cu(\mathbf{4})]^+$ was determined as log K = 2.81 ± 0.16 (ESI,† Fig. S26). We propose to denote the heteroleptic complexation motif between a $[Cu(phenAr_2)]^+$ and an alkyne as HETPYNE interaction (*vide supra*).

After establishing the HETPYNE motif, the zinc(II) porphyrin **3** with two ethynyl terminals was designed. To synthesize ligand **3**, we first reacted 5,15-di(4-iodophenyl)-10,20-dimesityl zinc(II) porphyrin and 4-ethynylphenol under Sonogashira coupling conditions providing the corresponding diphenol. In the final step, a Williamson ether synthesis between the phenol-substituted zinc(II) porphyrin and propargyl bromide in presence of base furnished ligand **3** in 85% yield. Protons e-H of **3** appear in the ^{1}H NMR well separated from other proton signals and should serve as good indicator of any binding.

As expected from the model studies, the four-component self-assembly **ASB-1** was quantitatively afforded by mixing DABCO, ligands **1** & **3**, and $[Cu(CH_3CN)_4]PF_6$ in a 1 : 1 : 1 : 2 ratio in CD_2Cl_2 (Fig. 3a). Two characteristic multiplets for the CH_2-units of DABCO in the negative region of the ^{1}H NMR indicated quantitative formation of the hetero-sandwich complex (Fig. 3b).[37] Significant changes at all phenanthroline protons in the ^{1}H NMR upon moving from $[Cu_2(\mathbf{1})]^{2+}$ to **ASB-1** supported the binding of **3** to the copper(I)-loaded phenanthroline stations (Fig. 3c and d). Downfield shift of proton f-H from 2.64 to 3.10 ppm in **ASB-1** attested the terminal ethynyl binding of **3** at the Cu^+ center of **1** (Fig. 3d). Drastic upfield shifts of proton signal e-H from 4.79 to 3.60 ppm and of d-H from 7.05 to 6.77 ppm along with a downfield shift of proton signal c-H from 7.64 to 7.75 ppm validated the formation of the HETPYNE complex. Furthermore, a single peak in the ESI-MS at m/z = 1489.1 confirmed formation of the hetero-assembly (ESI,† Fig. S23) and a single diffusion trace in the ^{1}H-DOSY NMR representing structure **ASB-1** excluded the presence of other undesired assemblies (ESI,† Fig. S20).

The clean formation of the heteroleptic sandwich complex encouraged us to test the HETPYNE motif as a dynamic interaction in a multicomponent rotor. To assemble the rotor, we selected zinc(II) porphyrin **2** containing just one phenanthroline station as stator and ligand **3** as rotator. Dissolving the ligands **2**, **3**, DABCO and $[Cu(CH_3CN)_4]PF_6$ in a 1 : 1 : 1 : 1 ratio in CD_2Cl_2 quantitatively furnished rotor **ROT-1** irrespective of the sequence of addition (Fig. 4a). As in **ASB-1**, two broad signals in the negative region corresponding to DABCO and significant shifts of all phenanthroline protons in the ^{1}H NMR validated formation of the heteroassembly (Fig. 4b–d). Upfield shifts of rotator proton signals e-H from 4.79 to 4.19 ppm along with downfield shift of f-H from 2.64 to 2.88 ppm authenticated the rotor structure (Fig. 4c and d). Its formation was further confirmed by DOSY NMR and ESI-MS data (ESI,† Fig. S21 and S24).

A single set of ^{1}H NMR signals for protons c-H, d-H, e-H and f-H of **ROT-1** suggested fast rotation of the rotor on the NMR

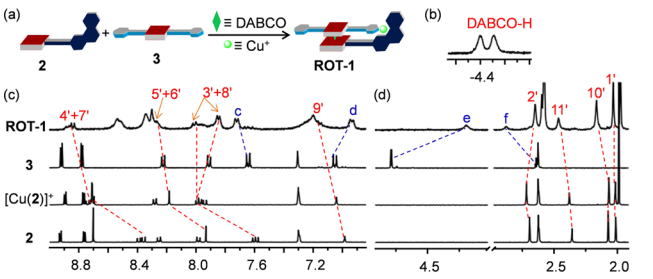

Fig. 4 (a) Cartoon representation of the self-assembly of rotor **ROT-1** from four components. (b) $(CH_2)_{DABCO}$ signal of **ROT-1** in the ^{1}H NMR (CD_2Cl_2, 400 MHz). Partial ^{1}H NMR (CD_2Cl_2, 400 MHz, 298 K) of **2**, $[Cu(\mathbf{2})]^+$, **3** and **ROT-1** in the (c) aromatic and (d) aliphatic region.

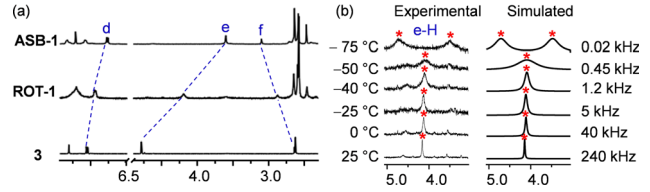

Fig. 5 (a) Partial ^{1}H NMR (CD_2Cl_2, 400 MHz, 298 K) of **3**, **ROT-1** and **ASB-1**. (b) VT-^{1}H NMR (CD_2Cl_2, 600 MHz) of **ROT-1** exhibiting the splitting of proton signal e-H into a 1 : 1 set and the corresponding rotational frequency at different temperatures.

time scale (Fig. 4c and d). Comparison of the ^{1}H NMR spectra of the free rotator **3**, **ROT-1** and **ASB-1** showed that the proton signals d-H, e-H and f-H of rotor **ROT-1** appeared approximately in the averaged position of those of free **3** and **ASB-1** (Fig. 5a). Variable temperature (VT) ^{1}H NMR of **ROT-1** was thus performed to evaluate its dynamic behavior. Upon lowering the temperature, the sharp singlet at 4.19 ppm corresponding to proton e-H broadened and split into two singlets in a 1 : 1 ratio at −75 °C with a coalescence temperature around −50 °C (Fig. 5b). The upfield signal at 3.50 ppm was assigned to the HETPYNE-complexed proton e-H and the downfield signal at 4.71 ppm is ascribed to proton e-H at the uncomplexed arm. The rotational frequency of the rotor at different temperatures was evaluated using winDNMR-based spectral simulations.[38] The activation data for the rotation was derived from the Eyring plot (Table 1 and ESI,† Fig. S18). The rotational frequency turned out to be 240 kHz at 25 °C and $\Delta G^{\ddagger}_{298}$ = 42.5 kJ mol^{-1}.

After the clean formation of rotor **ROT-1**, our next target was the *in situ* rotor-to-rotor transformation. The presence of a copper(I) ion and terminal alkynes in the rotor suggested a conversion of **ROT-1** to a triazole rotor through an *in situ* click reaction. For this purpose, 2.0 equiv. of benzyl azide was added to **ROT-1** in CD_2Cl_2 (Fig. 6a). To accelerate the reaction, 1 μL of Et_3N was added. After 24 h of heating at 40 °C, the solvent was evaporated to remove NEt_3 and the residue was redissolved in CD_2Cl_2. ^{1}H NMR showed quantitative formation of **ROT-2** and a disappearance of the proton signal f-H (Fig. 6b). Upon moving from **ROT-1** to **ROT-2**, characteristic shifts for all phenanthroline protons were observed. The downfield shift of proton signal e-H (from 4.19 to 4.81 ppm), upfield shifts of proton signals d-H (from 6.93 to 6.78 ppm) and c-H (from 7.72 ppm to 7.61 ppm) along with the appearance of a new singlet at 5.52 ppm (j-H) corroborated the formation of **ROT-2**. The broad signal of the DABCO protons at −4.39 ppm confirmed the

Table 1 Exchange frequencies of **ROT-1** and **ROT-2** along with their activation parameters[a]

Rotor	k_{298}/kHz	$\Delta H^{\ddagger}$/kJ mol^{-1}	$\Delta S^{\ddagger}$/J K^{-1} mol^{-1}	$\Delta G^{\ddagger}_{298}$/kJ mol^{-1}
ROT-1	240	44.0 ± 0.2	5.0 ± 0.7	42.5
ROT-2	77	50.1 ± 0.4	16.7 ± 0.6	45.2

[a] The higher $\Delta H^{\ddagger}$ for **ROT-2** than **ROT-1** reflects the stronger binding constant of a triazole to [Cu(**4**)]$^+$ (see triazole **6** in ESI, Fig. S27). As often seen in enthalpy–entropy compensation, strong binding leads to higher positive activation entropy.

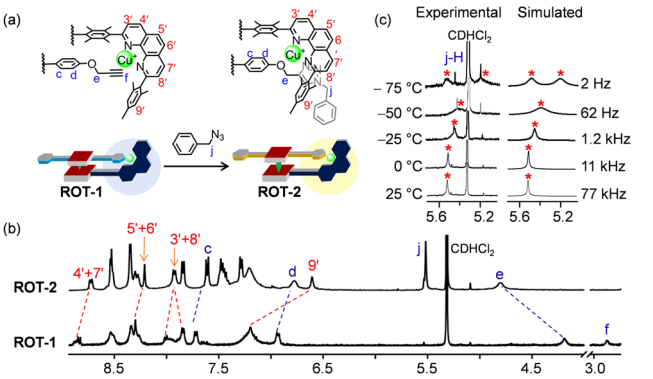

Fig. 6 (a) *In situ* transformation of **ROT-1** to **ROT-2** upon addition of 2.0 equiv. of benzyl azide. (b) Partial ^{1}H NMR (CD_2Cl_2, 400 MHz, 298 K) of **ROT-1** and **ROT-2**. (c) VT-^{1}H NMR (CD_2Cl_2, 600 MHz) of **ROT-2** showing splitting of the proton signal j-H (1 : 1 ratio) and the corresponding rotational frequency at different temperatures.

intactness of the assembly (ESI,† Fig. S15). **ROT-2** was further characterized by ESI-MS and DOSY NMR data (ESI,† Fig. S25 and S22).

A single set of ^{1}H NMR signals for protons c-H, d-H, e-H and j-H of **ROT-2** indicated a fast rotation on the NMR time scale. Upon performing the VT ^{1}H NMR the proton signal for j-H split into two singlets in 1 : 1 ratio at −75 °C (Fig. 6c). Rotational frequencies at different temperature along with activation parameters were calculated (Fig. 6c and Table 1). The facile transformation of the self-catalyzing rotor **ROT-1** to rotor **ROT-2** opens interesting perspectives to generate biohybrid materials *via* bioorthogonal click reactions.[39]

In conclusion, we have synthesized a four-component hetero-sandwich complex and a four-component rotor based on the dynamic [Cu(phenAr$_2$)(alkyne)]$^+$ motif. Though alkyne → copper(I) interactions are well known in the literature,[40] for the first time its high dynamics has been determined and used to assemble a high-speed multicomponent rotor. The utility of this dynamic orthogonal motif in supramolecular rotors opens new venues for molecular machines. Furthermore, a successful quantitative transformation of the Cu$^+$-alkyne rotor to a new Cu$^+$-triazole rotor was achieved through *in situ* click reaction. It is expected that thermal self-catalyzing rotors will find their way into diverse applications, *e.g.*, in catalysis,[35,41] biohybrid materials *via* bioorthogonal functionalization[42] and elsewhere.[43]

We are indebted to the Deutsche Forschungsgemeinschaft for continued support under Schm 647/22-1 (No 491092614). We thank Dr Paululat for measuring the VT-^{1}H NMR.

Conflicts of interest

There are no conflicts to declare.

Notes and references

1 M. Dutta and B. Jana, *Chem. Commun.*, 2021, **57**, 272–283.
2 J. E. Walker, *Biochem. Soc. Trans.*, 2013, **41**, 1–16.
3 R. D. Vale and R. A. Milligan, *Science*, 2000, **288**, 88–95.

4 H. Noji, R. Yasuda, M. Yoshida and K. Kinosita, Jr, *Nature*, 1997, **386**, 299–302.
5 A. Goswami, S. Saha, P. Biswas and M. Schmittel, *Chem. Rev.*, 2020, **120**, 125–199.
6 S. Kassem, T. van Leeuwen, A. S. Lubbe, M. R. Wilson, B. L. Feringa and D. A. Leigh, *Chem. Soc. Rev.*, 2017, **46**, 2592–2621.
7 S. Erbas-Cakmak, D. A. Leigh, C. T. McTernan and A. L. Nussbaumer, *Chem. Rev.*, 2015, **115**, 10081–10206.
8 A. J. McConnell, C. S. Wood, P. P. Neelakandan and J. R. Nitschke, *Chem. Rev.*, 2015, **115**, 7729–7793.
9 S. Kassem, T. van Leeuwen, A. S. Lubbe, M. R. Wilson, B. L. Feringa and D. A. Leigh, *Chem. Soc. Rev.*, 2017, **46**, 2592–2621.
10 Y. Feng, M. Ovalle, J. S. W. Seale, C. K. Lee, D. J. Kim, R. D. Astumian and J. F. Stoddart, *J. Am. Chem. Soc.*, 2021, **143**, 5569–5591.
11 M. Baroncini, S. Silvi and A. Credi, *Chem. Rev.*, 2020, **120**, 200–268.
12 B. Lin, I. Karki, P. J. Pellechia and K. D. Shimizu, *Chem. Commun.*, 2022, **58**, 5869–5872.
13 T. Kumpulainen, M. R. Panman, B. H. Bakker, M. Hilbers, S. Woutersen and A. M. Brouwer, *J. Am. Chem. Soc.*, 2019, **141**, 19118–19129.
14 H. V. Schröder, F. Stein, J. M. Wollschläger, S. Sobottka, M. Gaedke, B. Sarkar and C. A. Schalley, *Angew. Chem., Int. Ed.*, 2019, **58**, 3496–3500.
15 J. E. M. Lewis, R. J. Bordoli, M. Denis, C. J. Fletcher, M. Galli, E. A. Neal, E. M. Rochette and S. M. Goldup, *Chem. Sci.*, 2016, **7**, 3154–3161.
16 B. Doistau, L. Benda, J.-L. Cantin, L.-M. Chamoreau, E. Ruiz, V. Marvaud, B. Hasenknopf and G. Vives, *J. Am. Chem. Soc.*, 2017, **139**, 9213–9220.
17 H. Yoon, J. M. Lim, H.-C. Gee, C.-H. Lee, Y.-H. Jeong, D. Kim and W.-D. Jang, *J. Am. Chem. Soc.*, 2014, **136**, 1672–1679.
18 A. Petitjean, R. G. Khoury, N. Kyritsakas and J.-M. Lehn, *J. Am. Chem. Soc.*, 2004, **126**, 6637–6647.
19 B. Godde, A. Jouaiti, A. Fluck, N. Kyritsakas, M. Mauro and M. W. Hosseini, *Dalton Trans.*, 2017, **46**, 14897–14906.
20 M. C. Jimenez, C. O. Dietrich-Buchecker and J.-P. Sauvage, *Angew. Chem., Int. Ed.*, 2000, **39**, 3284–3287.
21 J. D. Badjic, V. Balzani, A. Credi, S. Silvi and J. F. Stoddart, *Science*, 2004, **303**, 1845–1849.
22 M. von Delius, E. M. Geertsema and D. A. Leigh, *Nat. Chem.*, 2010, **2**, 96–101.
23 M. Schmittel, *Chem. Commun.*, 2015, **51**, 14956–14968.
24 M. Schmittel, *Isr. J. Chem.*, 2018, **59**, 197–208.
25 P. K. Biswas, S. Saha, Y. Nanaji, A. Rana and M. Schmittel, *Inorg. Chem.*, 2017, **56**, 6662–6670.
26 B. E. Dial, P. J. Pellechia, M. D. Smith and K. D. Shimizu, *J. Am. Chem. Soc.*, 2012, **134**, 3675–3678.
27 S. Saha, P. K. Biswas and M. Schmittel, *Inorg. Chem.*, 2019, **58**, 3466–3472.
28 P. K. Biswas, A. Goswami, S. Saha and M. Schmittel, *Chem. – Eur. J.*, 2020, **26**, 14095–14099.
29 I. Paul, A. Goswami, N. Mittal and M. Schmittel, *Angew. Chem., Int. Ed.*, 2018, **57**, 354–358.
30 S. Hiraoka, M. Shiro and M. Shionoya, *J. Am. Chem. Soc.*, 2004, **126**, 1214–1218.
31 D. Parasar, T. T. Ponduru, A. Noonikara-Poyil, N. B. Jayaratna and H. V. R. Dias, *Dalton Trans.*, 2019, **48**, 15782–15794.
32 H. V. R. Dias, J. A. Flores, J. Wu and P. Kroll, *J. Am. Chem. Soc.*, 2009, **131**, 11249–11255.
33 S. K. Samanta and M. Schmittel, *J. Am. Chem. Soc.*, 2013, **135**, 18794–18797.
34 B. Ralahy, U. Hahn, E. Wasielewski and J.-F. Nierengarten, *Eur. J. Inorg. Chem.*, 2021, 2625–2635.
35 S. Saha, A. Ghosh, T. Paululat and M. Schmittel, *Dalton Trans.*, 2020, **49**, 8693–8700.
36 S. De, S. Pramanik and M. Schmittel, *Angew. Chem., Int. Ed.*, 2014, **53**, 14255–14259.
37 S. K. Samanta, D. Samanta, J. W. Bats and M. Schmittel, *J. Org. Chem.*, 2011, **76**, 7466–7473.
38 H. J. Reich, *NMR Spectrum Calculations: WinDNMR, Version 7.1.13*, Department of Chemistry, University of Wisconsin, 2008.
39 C. G. Parker and M. R. Pratt, *Cell*, 2020, **180**, 605–632.
40 M. Meldal and C. W. Tornøe, *Chem. Rev.*, 2008, **108**, 2952–3015.
41 A. Goswami, T. Paululat and M. Schmittel, *J. Am. Chem. Soc.*, 2019, **141**, 15656–15663.
42 **https://www.nobelprize.org/uploads/2022/10/popular-chemistryprize2022.pdf**.
43 K. T. Fam, L. Saladin, A. S. Klymchenko and M. Collot, *Chem. Commun.*, 2021, **57**, 4807–4810.